Mutational Analysis of Active Site Residues in the *Staphylococcus aureus* Transpeptidase SrtA†

Brenda A. Frankel,‡ Yan Tong,§ Matthew L. Bentley,‡ Michael C. Fitzgerald,§ and Dewey G. McCafferty*,‡,§

Department of Biochemistry and Biophysics and the Johnson Research Foundation, The University of Pennsylvania School of Medicine, Philadelphia, Pennsylvania 19104, and Department of Chemistry, Duke University, Durham, North Carolina 27708

Received March 6, 2007

ABSTRACT: In *Staphylococcus aureus*, virulence and colonization-associated surface proteins are covalently anchored to the cell wall by the transpeptidase Sortase A (SrtA). In order to better understand the contribution of specific active site residues to substrate recognition and catalysis, we performed mutational analysis of several key residues in the SrtA active site. Analysis of protein stability, kinetic parameters, solvent isotope effects, and pH−rate profiles for key SrtA variants are consistent with a reverse protonated Cys184-His120 catalytic dyad, and implicate a role for Arg197 in formation of an oxyanion hole to stabilize the transition state. In contrast, mutation of Asp185 and Asp186 produced negligible effects on catalysis, and no evidence was found to support the existence of a functional catalytic triad. Mutation of Thr180, Leu181, and Ile182 to alanine produced modest decreases in SrtA activity and led to substrate inhibition. Thermodynamic stability measurements by SUPREX (stability of unpurified proteins from rates of H/D exchange) revealed decreases in conformational stability that correlate with the observed substrate inhibition for each variant, signifying a potential role for the conserved ^{180}TLITC^{184} motif in defining the active-site architecture of SrtA. In contrast, mutation of Thr183 to alanine led to a significant 1200-fold decrease in k_{cat}, which appears to be unrelated to conformational stability. Potential explanations for these results are discussed, and a revised model for SrtA catalysis is presented.

The ubiquitous role of sortase transpeptidases in mediating the pathogenesis of Gram-positive pathogens such as *Staphylococcus aureus* by catalyzing the attachment of surface protein virulence factors to the cell-wall peptidoglycan layer is well-established (*1*). For this reason, inhibition of surface protein anchoring by targeting the sortase reaction is an attractive approach for the development of novel anti-infective chemotherapeutics with activity against multiply drug resistant strains of Gram-positive bacteria such as MRSA[1] and VRSA. Despite the recognized potential of *S. aureus* SrtA as a target for antibacterial action, efforts to develop potent and selective inhibitors of the sortase reaction have yet to yield any promising candidates for clinical use. This shortcoming is largely the consequence of our poor understanding of SrtA mechanism and substrate recognition.

Recombinant SrtA catalyzes the in vitro transpeptidation of LPXTG-containing peptides with a pentaglycine peptidoglycan mimic through a ping-pong mechanism with a partial hydrolytic shunt (*2*, *3*). Transpeptidation proceeds through acylation of the SrtA active-site nucleophile Cys184 which has been demonstrated through site-directed mutagenesis and chemical modification to be essential for catalysis (*4*). The initial NMR structural determination of the SrtA active site revealed a potential Cys-His-Asn catalytic triad reminiscent of the cysteine protease papain (*5*). Subsequent site-directed mutagenesis demonstrated the catalytic requirement for the absolutely conserved His120 and in contrast indicated that Asn98 was dispensable for SrtA activity (*4*, *6*).

Although SrtA activity studies continue to support the critical involvement of His120 in catalysis, more recent X-ray crystallographic structures of *S. aureus* SrtA and SrtB have raised the possibility of a central role for Arg197 in catalysis, whereas the side chain of His120 appears to be far-removed from the site of chemistry (*7*, *8*). Accordingly, site-directed mutagenesis of Arg197 to alanine or lysine resulted in a 1500-fold decrease in k_{cat} while K_m was largely unaffected and led Marraffini et al. to propose a general base role for Arg197 in modulating the ionization state of Cys184 (*6*). However, the observed effects of Arg197 mutation on SrtA catalysis may be more consistent with a role in stabilizing the oxyanion transition state preceding acyl-enzyme formation, as has been observed for carboxypeptidase A and cytomegalovirus protease (*9*, *10*).

† This work was supported by NIH Grant AI46611 to D.G.M. and a NSF Graduate Research Fellowship to B.A.F.

* To whom correspondence should be addressed: Department of Chemistry, Duke University, B120 LSRC Building, Box 90317, Durham, NC 27708-0317. Tel: 919-660-1516: Fax: 919-668-5483: E-mail: dewey@duke.edu.

‡ University of Pennsylvania School of Medicine.

§ Duke University.

[1] Abbreviations: MRSA, methicillin-resistant *Staphylococcus aureus*; VRSA, vancomycin-resistant *Staphylococcus aureus*; SUPREX, stability of unpurified proteins from rates of H/D exchange; Dap, diaminopropionic acid; Dnp, dinitrophenol; Abz, aminobenzoic acid; CD, circular dichroism; TFA, trifluoroacetic acid; HPLC, high-pressure liquid chromatography; DMSO, dimethyl sulfoxide; PCR, polymerase chain reaction; MALDI-MS, matrix assisted laser desorption ionization mass spectrometry.

10.1021/bi700448e CCC: $37.00
Published on Web 05/23/2007

In addition to the controversy surrounding the catalytic mechanism of SrtA we also have very limited knowledge of the structural basis for substrate specificity. *S. aureus* SrtA recognizes and cleaves the LPXTG motif with a very high degree of specificity, and only a few conservative substitutions are tolerated in this recognition motif (*11*). Similarly, *S. aureus* SrtB is known to recognize and cleave only NPQTN-containing substrates and no cross-talk between SrtA and SrtB processing has been observed *in vitro* or *in vivo* (*12*). Recently, two groups independently identified the $\beta6-\beta7$ loop of SrtA and the underlying β-sheet formed by the $\beta4$, $\beta7$, and $\beta8$ strands as the primary interaction surface of the LPXTG motif with SrtA (*7*, *13*). Leu and Pro make hydrophobic contacts along the $\beta7$ strand, and Thr is positioned proximally to Cys184. All sortase isoforms contain a conserved active site TLXTC motif, which in SrtA is located along the $\beta7$ strand spanning residues 180 to 184 (*14*). It is therefore interesting to speculate that this sequence might contribute to the substrate selectivity of sortase enzymes by participating in binding or recognizing the LPXTG motif. In *S. aureus* SrtA, the cysteine residue of this motif has been well-characterized as the active-site nucleophile required for catalysis, mutation of Thr180 to lysine had a minimal effect on SrtA catalysis, and no activity was detected after mutation of Ile182 to serine, the corresponding residue in SrtB isoforms (*13*, *15*). However, no quantitative analysis has been performed and the potential roles of Leu181 and Thr183 have yet to be examined.

Recent advances in characterizing the molecular basis for SrtA catalysis and substrate specificity have provided a platform for a more rationally guided search for effective sortase inhibitors. However, many questions remain unanswered. pH−rate profile and isotope effect studies performed with wild-type SrtA support a reverse protonation model for SrtA catalysis in which, at physiological pH, only a small fraction of SrtA exists in an active form with Cys184 thiolate and His120 imidazolium (*2*). However, these studies fail to account for the demonstrated role of Arg197 in catalysis and do not adequately examine the potential involvement of aspartate residues present at positions 185 and 186 in SrtA. Furthermore, the sortase field demonstrably suffers from a lack of specific knowledge regarding the molecular basis for the exquisite substrate selectivity of sortase transpeptidases. In the current study we begin to address these issues through site-directed mutagenesis of SrtA active-site residues hypothesized to be involved in catalysis and substrate binding. Herein we report the effects of active SrtA variants on the kinetic parameters k_{cat} and K_m as well as the effect of these mutations on structural stability. For several key variants the pH-dependence and solvent isotope effects on catalysis were evaluated. Finally, we discuss implications of these results with respect to the catalytic mechanism of SrtA.

MATERIALS AND METHODS

General. Buffer salts were purchased from Sigma. D_2O was purchased from Aldrich. Standard Fmoc amino acids (Novabiochem), Fmoc-Dap(Dnp)-OH (Bachem), NH_2-Gly_5-OH (Bachem) were purchased and used without further purification. Solid-phase synthesis of Abz-LPETG-Dap-(Dnp)-NH_2 was performed with an Applied Biosystems 433A synthesizer. Gel filtration chromatography was performed on a Biocad Sprint chromatography system (Applied Biosystems). HPLC was performed using a Thermo Separation Products SpectraSYSTEM equipped with an autosampler and either a semipreparative Jupiter octadecyl silica column (Phenomenex) or a fast analytical (4.6 mm × 50 mm, 3 μm) octadecyl silica column (Vydac).

Table 1: Primer Sequences for SrtA Mutagenesis

Mutation	Primer Sequences 5' → 3'[a]
H120A	TCAATTGCAGGAGCCACTTTCATTGAC
	GTCAATGAAAGTGGCTCCTGCAATTGA
H120Q	TCAATTGCAGGACAAACTTTCATTGAC
	GTCAATGAAAGTTTGTCCTGCAATTGA
T180A	GATAAACAATTAGCATTAATTACTTGTG
	CACAAGTAATTAATGCTAATTGTTTATC
L181A	GATAAACAATTAACAGCAATTACTTGTGATG
	CATCACAAGTAATTGCTGTTAATTGTTTATC
I182A	CAATTAACATTAGCTACTTGTGATGATTAC
	GTAATCATCACAAGTAGCTAATGTTAATTG
I182S	CAATTAACATTAAGTACTTGTGATGATTAC
	GTAATCATCACAAGTACTTAATGTTAATTG
T183A	CAATTAACATTAATTGCTTGTGATGATTAC
	GTAATCATCACAAGCAATTAATGTTAATTG
C184A	CATTAATTACTGCTGATGATTACAATG
	CATTGTAATCATCAGCAGTAATTAATG
C184H	CATTAATTACTCATGATGATTACAATG
	CATTGTAATCATCATGAGTAATTAATG
C184S	CATTAATTACTAGTGATGATTACAATG
	CATTGTAATCATCACTAGTAATTAATG
D185A	CATTAATTACTTGTGCTGATTACAATGAAAAG
	CTTTTCATTGTAATCAGCACAAGTAATTAA
D186A	CATTAATTACTTGTGATGCTTACAATGAAAAG
	CTTTTCATTGTAAGCATCACAAGTAATTAATG
R197A	GTTTGGGAAAAAGCTAAAATCTTTGTAGC
	GCTACAAAGATTTTAGCTTTTTCCCAAAC
R197K	GTTTGGGAAAAAAAAAAAATCTTTGTAGC
	GCTACAAAGATTTTTTTTTTTTCCCAAAC

[a] Mutated codons are underlined.

Site-Directed Mutagenesis. The expression plasmid pET15b$SrtA_{\Delta N24}$ encoding wild-type His_6-$SrtA_{\Delta N24}$ (*11*) served as a template for the introduction of single amino acid substitutions by PCR using the QuikChange method (Stratagene). All PCR reactions contained DMSO (5%). The complementary forward and reverse primer pairs employed to construct each SrtA variant discussed are listed in Table 1. Mutational changes were confirmed by DNA sequencing.

Expression and Purification of Wild-Type and Mutant SrtA. Expression of wild-type and variant SrtA was performed as described previously (*2*). For purification, cell pellets from 1 L of culture were resuspended in equilibration buffer (150 mM NaCl, 50 mM Tris, 5 mM imidazole, 10% glycerol, pH 7.5) and lysed using an EmulsiFlex-C5 high-pressure homogenizer (Avestin, Inc.). The resultant lysate was clarified by centrifugation and incubated on ice with 4 to 5 mL of chelating sepharose (Pharmacia Biotech) for 30 min to 1 h. The lysate−resin mixture was then applied to a benchtop gravity flow column, and the flow-through was reapplied to the column bed. The column was washed twice with ice-cold equilibration buffer (30 mL) and another two times with the same buffer containing 20 mM imidazole. Elution was achieved with four applications (8 mL) of the same buffer containing 200 mM imidazole. The first two elution fractions, holding the majority (>98%) of SrtA, were pooled and concentrated to a volume of 8−12 mL using Centriplus YM-10 concentrators (Millipore). The concentrated eluant was then loaded at 1 mL/min onto a HiPrep 26/60 Sephacryl S-200 gel filtration column (Pharmacia Biotech) pre-equilibrated with gel filtration buffer (150 mM NaCl, 50 mM Tris, 5 mM $CaCl_2$, 0.1% β-mercaptoethanol,

10% glycerol, pH 7.5). β-Mercaptoethanol was omitted during the purification of the Cys184 mutants. Generally, two 8 mL fractions containing pure SrtA were pooled and concentrated to at least 300 μM using a Centriplus YM-10 concentrator. The concentration of wild-type and mutant SrtA was determined using the calculated extinction coefficient $\epsilon_{280} = 17420\ M^{-1}\ cm^{-1}$ (*16*).

Circular Dichroism Spectroscopy. To reduce salt and buffer concentrations, aliquots (100 to 300 μL) of wild-type and mutant SrtA were dialyzed against buffer containing Tris (25 mM, pH 7.5), $CaCl_2$ (5 mM), and NaCl (75 mM). Dialyzed SrtA was combined in a total volume of 20 μL with Na phosphate (10 mM, pH 7.5) resulting in samples with protein concentration ranging from 7.7 to 10.6 μM in a total volume of 0.5 mL. For each SrtA mutant 250 μL was transferred to a quartz cuvette with 0.1 cm path length for CD data collection. CD spectra were measured using a JASCO J-810 CD spectrometer equipped with a six-cell holder. Data were collected at 25 °C from 260 to 190 nM in step mode with a scanning speed of 4 s/nm. For each sample three scans were averaged and corrected for background absorbance. The observed CD signal was converted to mean residue ellipticity (θ, deg cm^2 $dmol^{-1}$ $residue^{-1}$) using eq 1:

$$\theta = \theta_{obs}/10(cdn) \quad (1)$$

where θ_{obs} is the observed ellipticity in degrees, c is the protein concentration in mol/L, d is the optical path length in cm, and n is the number of amino acid residues in the protein (202 for His_6-$SrtA_{\Delta N24}$ and mutants).

Thermodynamic Measurements Using SUPREX. SUPREX analyses on SrtA and variants were performed using data acquisition and analysis protocols that have been previously described (*17*). Briefly, protein solutions (2 mg/mL) of fully protonated SrtA were diluted 10-fold into a series of deuterated H/D exchange buffers (20 mM sodium phosphate, 100 mM KCl, 0 to 5.5 M urea, pD 7.5) to initialize H/D exchange. Following a 23 h exchange period, aliquots from each H/D exchange reaction were quenched by 10-fold dilution into an ice-cold MALDI matrix solution consisting of saturated sinapinic acid, 45% acetonitrile, and 0.1% TFA.

A 1−2 μL aliquot of each quenched H/D exchange reaction was deposited onto a MALDI sample plate, and the sample was subjected to MALDI-MS analysis. Mass spectra were acquired on a Perseptive Biosystems Voyager DE Biospectrometry Workstation. Cytochrome *c* (MW 12,361.1 Da) and trypsin inhibitor (MW 19,979.6 Da) were used as internal calibration standards. Positive ion mass spectra were collected in the linear mode using a nitrogen laser (337 nm, 3 Hz). Each spectrum collected was the sum of data from 32 laser shots. ΔMass values were calculated by subtracting the molecular weight of fully protonated SrtA from the mass measured in each MALDI analysis. The Δmass values calculated from five replicate measurements were averaged and plotted as a function of urea concentration. The data were fit to a four-parameter sigmoidal curve using SigmaPlot (SYSTAT Software Inc.) to determine $C^{1/2}_{SUPREX}$, the denaturant concentration at the transition midpoint.

Sortase Activity Measurements. In initial tests, wild-type (1 μM) and mutant (1, 50, or 200 μM) SrtA were assayed for activity in the HPLC assay described previously with the peptide substrates Abz-LPETG-Dap(Dnp)-NH_2 (0.2−0.33 mM) and NH_2-Gly_5-OH (2 mM) (*18*). Assays were run for 30 min or overnight depending on activity level. For variant SrtA enzymes, initial estimates of fold activity decrease, compared to wild-type SrtA at the same substrate concentrations, were calculated as the ratio of wild-type to mutant activity after correcting for differences in enzyme concentration and assay time. When full kinetic analysis was possible for SrtA variants, the fold activity decrease estimated in this manner was found to correlate well with the relative reduction in k_{cat}/K_m. Therefore, these initial estimates were used to compare the relative activity of SrtA H120A and SrtA H120Q for which more precise measurements could not be obtained.

For subsequent measurement of kinetic parameters, concentrations and assay lengths for sortase variants were chosen to approximate activity levels observed for 1 μM wild-type enzyme in a 30 min reaction. Whenever possible, the volume of enzyme added to activity assays was limited to one-tenth of the total assay volume. The linearity of sortase activity was verified by analyzing product formation as a function of time over the selected interval. With the exception of enzyme concentration and assay time, all experiments were performed under the same conditions utilized for wild-type SrtA. Enzyme concentrations and assay lengths employed for each of the SrtA mutants were as follows: T180A, 1 μM for 5 or 5.5 h; L181A, 1 μM for 2.5 h; I182A, 20 μM for 30 min; I182S, 50 μM for 30 min; T183A, 100 μM for 5 h; C184S, 200 μM for 6 h; D185A and D186A, 1 μM for 30 min; R197A, 50 μM for 5 h; R197K, 100 μM for 5 h.

Abz-LPETG-Dap(Dnp)-NH_2 was typically varied over a a range of 0.27 to 23 mM, and Michaelis−Menten analysis was performed using GraFit (Erithacus Software) to obtain the parameters k_{cat} and K_m. For SrtA T180A, L181A, I182A, and I182S, k_{cat}/K_m ratios were calculated from the slopes of lines drawn through the data obtained at low Abz-LPETG-Dap(Dnp) concentrations: 0.33−7.9 mM for SrtA T180A, 0.29−2.3 mM for SrtA L181A, 0.3−9.5 mM for SrtA I182A, and 0.59−13.1 mM for SrtA I182S. In several cases, the change in free energy of the transition state for SrtA mutants was calculated from eq 2:

$$\Delta\Delta G^{\ddagger} = -RT \ln\left(\frac{(k_{cat}/K_m)_{Mut}}{(k_{cat}/K_m)_{WT}}\right) \quad (2)$$

where $\Delta\Delta G^{\ddagger}$ is the change in free energy of the transition state between wild-type (WT) and mutant (Mut), R is the ideal gas constant, and T is temperature.

pH-Dependence of k_{cat} for Wild-Type SrtA, SrtA C184S, SrtA R197A, and SrtA R197K. To examine the pH stability of wild-type SrtA, enzyme (10 μM) was preincubated in buffer A (50 mM acetic acid, 50 mM MES, 100 mM Tris, 5 mM $CaCl_2$, 150 mM NaCl) adjusted to pH 3.55−7.5, or buffer B (50 mM MES, 100 mM Tris, 50 mM CAPS, 5 mM $CaCl_2$, 150 mM NaCl) adjusted to pH 5.5−11.0, at 37 °C for 30 min, 5 h, or 6 h. SrtA activity was then assayed in duplicate with SrtA (1 μM) and Abz-LPETG-Dap(Dnp)-NH_2 (0.26 mM) in standard assay buffer (150 mM NaCl, 5 mM $CaCl_2$, and 300 mM Tris-Cl, pH 7.5).

k_{cat} measurements were made in buffer A or B with concentrations and assay times for each SrtA variant as indicated in the previous section. k_{cat} was determined by

measuring the rate of product formation in the presence of 10.5 mM Abz-LPETG-Dap(Dnp) for SrtA C184S, 15.6 mM for SrtA R197A, 16.7 mM for R197K, and 17.8 mM for wild-type SrtA. Due to poor substrate solubility at low pH and assay sensitivity limitations at high pH, k_{cat} was observable in the pH range from 5.0 to 10.5 for SrtA C184S, 5.5 to 10.0 for R197A and R197K variants, and 5.5 to 10.5 for wild-type SrtA. The data were modeled using GraFit (Erithacus) to eq 3 or 4 describing bell-shaped and single titrations respectively,

$$\log y_{obs} = \log\left(\frac{y_{max}}{1 + [H^+]/K_{a1} + K_{a2}/[H^+]}\right) \quad (3)$$

$$\log y_{obs} = \log\left(\frac{y_{max}}{1 + K_a/[H^+]}\right) \quad (4)$$

where y_{obs} is the measured parameter k_{cat}, y_{max} is the pH-independent value of k_{cat}, $[H^+]$ is the concentration of protons in solution, and $K_{a,}$ K_{a1}, and K_{a2} are the midpoints of the observed titrations.

Measurement of Solvent Isotope Effects for SrtA C184S, D185A, D186A, and R197A. The effect of substituting D_2O for H_2O in the reactions catalyzed by SrtA C184S, D185A, D186A, and R197A was measured on the kinetic parameters k_{cat} and k_{cat}/K_m. The SrtA substrates Abz-LPETG-Dap(Dnp) and Gly_5 were dissolved in D_2O prior to addition. Reaction buffers were prepared in H_2O, lyophilized to dryness, and redissolved in an equivalent volume of D_2O. Enzyme concentrations and assay times were as reported above. For SrtA C184S a titration of Abz-LPETG-Dap(Dnp) was performed in the presence of 88.5% D_2O, and kinetic parameters were obtained from Michaelis−Menten analysis. SrtA D185A and SrtA D186A were similarly examined in 99% D_2O. Reported isotope effects were calculated by dividing the value of the parameter measured in H_2O by that measured in D_2O. For SrtA R197A the kinetic parameters k_{cat} and k_{cat}/K_m were calculated from measurements at single concentrations of Abz-LPETG-Dap(Dnp), 20.3 mM for k_{cat} and 0.29 mM for k_{cat}/K_m. Measurements were performed in 90% D_2O and compared to values obtained by the same method in H_2O.

RESULTS AND DISCUSSION

Cloning, Expression, and Purification of Site-Specific SrtA Variants. To gain a detailed understanding of the SrtA catalytic mechanism and specific roles played by conserved residues in catalysis, we constructed a series of 14 site-specific amino acid substitutions in the SrtA sequence. In the first round of mutagenesis, residues previously implicated in SrtA catalysis were varied. Cys184 was mutated to alanine, histidine, and serine; His120 was mutated to both alanine and glutamine; Arg197 was mutated to both alanine and lysine; and Asp185 and Asp186 were mutated to alanine. In a second series of experiments we examined additional residues within the conserved active-site ^{180}TLITC^{184} motif that we hypothesized were likely to play a role in substrate binding and recognition. Thr180, Leu181, Ile182, and Thr183 were mutated to alanine; Ile182 was also mutated to serine, the corresponding amino acid in SrtB sortase isoforms (*15*). All mutants behaved similarly to wild-type SrtA throughout the purification process and were purified to >95% homogeneity as judged by SDS−PAGE (not shown).

Circular Dichroism Analysis of SrtA Mutant Structure. Altering the amino acid composition of a protein has the potential to produce changes in secondary structure and folding which may erroneously be interpreted as a direct effect on enzymatic catalysis. We therefore compared the CD spectra of each mutant to that of wild-type SrtA to determine if the mutations we introduced created any gross structural perturbations. Initially we assessed the appropriateness of CD as a technique to monitor changes in the secondary structure of wild-type SrtA. The CD spectra of wild-type SrtA collected at 25 °C and at 98 °C are shown in Figure 1A. Although the CD spectrum collected for wild-type SrtA at 25 °C lacks strong distinguishing features, the enzyme was found to be active under the conditions used for CD and is therefore assumed to be properly folded. When heat-denatured, the intensity of the CD signal generated by SrtA was reduced and the shape of the spectrum was visibly altered, verifying that global unfolding of SrtA is detectable by CD spectroscopy. CD data collected for the SrtA mutants is shown overlaid with the wild-type CD spectrum (Figure 1B−D). No gross structural perturbations were observed for any of the SrtA variants; however, it is important to note that this result does not rule out the possibility of changes in conformational stability.

SUPREX Analysis of Wild-Type SrtA and Variants. To evaluate potential effects of selected SrtA mutations on the conformational stability of the protein, we employed the SUPREX technique (*17*), which permits the acquisition of thermodynamic data on a protein under denaturant concentrations where the protein is predominantly folded. This technique was initially applied to wild-type SrtA. Figure 2 shows a typical SUPREX curve for wild-type SrtA obtained using an H/D exchange time of 23 h. At this exchange time, SrtA yielded a pretransition baseline of ~110 Da, a post-transition baseline of ~160 Da, and an amplitude of ~50 Da for the SUPREX transition. The sigmoidal curve in Figure 2 is indicative of a global unfolding event in the protein. In addition, the Δmass values of the post-transition region of the SUPREX curve (denaturant concentrations > 3 M) are in line with those expected for a 206 amino acid protein (M.C.F., unpublished observation). Thus, the midpoint of this transition (the $C^{1/2}_{SUPREX}$ value, which is defined as the concentration of denaturant at which the protein has exchanged half of its globally protected amide protons) can be used as a qualitative measure of the overall conformational stability of the protein.

In order to compare the conformational stability of SrtA mutants to the wild type, SUPREX analysis was carried out for 11 of the SrtA mutants discussed in this study (Table 2). $C^{1/2}_{SUPREX}$ values obtained under the same SUPREX conditions (i.e., the same buffer composition and 23 h H/D exchange time) were used to compare the conformational stabilities of the mutants to the wild type. For the majority of the mutants no significant change in $C^{1/2}_{SUPREX}$ was observed, suggesting that most of the mutations did not affect the conformational stability of SrtA. For mutations T180A, L182A, I182A, and I182S, the $C^{1/2}_{SUPREX}$ values were decreased, as compared to the wild type. This suggests that mutation of these residues leads to conformational destabi-

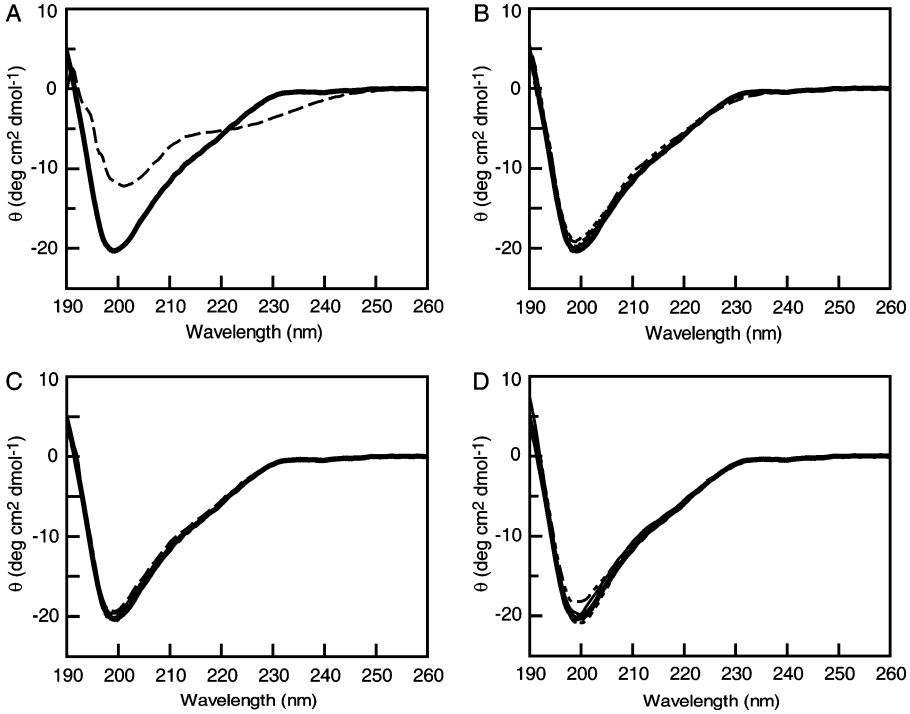

FIGURE 1: CD spectra for wild-type and variant SrtA enzymes. Spectra were measured in 10 mM phosphate, pH 7.5. Mean residue ellipticity (θ), as calculated from eq 1, is plotted as a function of wavelength. (A) CD spectra for wild-type SrtA were measured at 25 °C (solid) and at 98 °C (dash). (B) CD spectra of C184A (solid), C184H (dash), C184S (dot), R197A (dash-dot-dash), and R197K (dash-dot−dot) are overlaid with that of wild-type SrtA (bold). (C) CD spectra of H120A (solid), H120Q (dash), D185A (dot), and D186A (dash-dot-dash) are overlaid with that of wild-type SrtA (bold). (D) CD spectra of T180A (solid), L181A (dash), I182A (dot), I182S (dash-dot-dash), and T183A (dash-dot−dot) are overlaid with that of wild-type SrtA (bold).

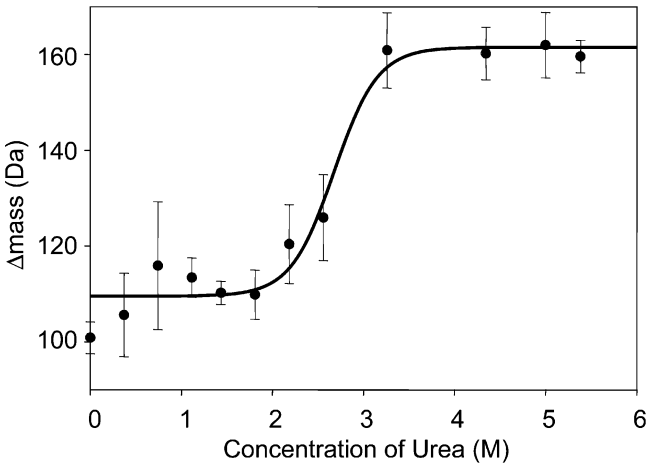

FIGURE 2: SUPREX curve obtained for wild-type SrtA. The amide H/D exchange time was 23 h. The Δmass values are the average of 5 replicate values determined from 5 replicate MALDI mass spectra. The line represents the best fit of the data to a sigmoidal equation (see text). The transition midpoint (i.e., the $C^{1/2}_{SUPREX}$ value) is indicated with an arrow. The error bars represent ±1 standard deviation.

lization of the protein, with a concomitant decrease in catalytic activity (Table 3).

Effects of Mutating H120, C184, D185, D186, and R197 on SrtA Catalysis. The SrtA residues His120, Cys184, Asp185, Asp186, and Arg197 were initially examined by site-directed mutagenesis on the basis of their previously proposed roles in SrtA catalysis. Kinetic parameters and calculations of $\Delta\Delta G^{\ddagger}$ for all mutants with measurable activity are compared in Table 3.

In an initial assessment of SrtA H120A and SrtA H120Q activity estimated decreases of 96,000- or 36,000-fold in enzymatic activity were calculated relative to wild-type SrtA, respectively. Unfortunately, the level of activity for both variants was too low to obtain more precise measurements. However, it is interesting to note that the detection of activity for SrtA H120A is contradictory to the earlier observation of Ton-That et al. that mutation of His120 to alanine resulted in complete loss of product formation (*4*). In addition, the 3-fold higher activity measured for the conservative SrtA H120Q mutation compared to H120A suggests that this finding is not attributable to experimental artifact. Due to our inability to individually determine k_{cat} and K_m for SrtA H120A and SrtA H120Q, we used initial estimates of fold activity decrease for comparison to k_{cat}/K_m values of the remaining mutants. The estimated 10^4-fold reduction in catalytic efficiency for these variants is consistent with the participation of His120 as an acid or base in SrtA catalysis as it represents the largest decrease in SrtA activity observed in this study.

In accordance with previous findings, mutation of Cys184 to alanine or histidine completely abolished the catalytic activity of SrtA as expected for mutation of the active-site

Table 2: Summary of Transition Midpoints ($C^{1/2}_{SUPREX}$ Values) Obtained by SUPREX Analysis of SrtA and SrtA Variants, Using H/D Exchange Time of 23 h

SrtA variant	$C^{1/2}_{SUPREX}$ (M)[a]	SrtA variant	$C^{1/2}_{SUPREX}$ (M)[a]
wild-type	2.6	I182S	1.3
H120A	2.6	T183A	2.7
H120Q	2.6	D185A	2.6
T180A	1.6	D186A	2.7
L181A	0.8	R197A	2.4
I182A	1.5	R197K	2.3

[a] Standard deviations for $C^{1/2}_{SUPREX}$ are typically 0.1 M.

Table 3: Kinetic Analysis of SrtA Mutants

enzyme	k_{cat} (s^{-1})	K_m (mM)	k_{cat}/K_m (M^{-1} s^{-1})	fold act. decrease[a]	$\Delta\Delta G^{\ddagger}$(kcal/mol)[b]
wild type	0.69 ± 0.01	10.6 ± 0.5	64.5		
H120A	nd[c]	nd	nd	9.6×10^4	6.8
H120Q	nd	nd	nd	3.6×10^4	6.2
T180A	nd	nd	4.5	14	1.6
L181A	nd	nd	8.5	7.6	1.2
I182A	nd	nd	2.3	28	2.0
I182S	nd	nd	0.87	74	2.6
T183A	$6.0 \times 10^{-4} \pm 0.1 \times 10^{-4}$	11.2 ± 0.5	0.054	1.2×10^3	4.2
C184S	$1.9 \times 10^{-5} \pm 0.03 \times 10^{-5}$	0.79 ± 0.07	0.024	2.7×10^3	4.7
D185A	0.72 ± 0.02	8.5 ± 0.6	84.7		
D186A	0.78 ± 0.02	6.7 ± 0.4	116		
R197A	$4.6 \times 10^{-4} \pm 0.2 \times 10^{-4}$	3.8 ± 0.4	0.12	5.4×10^2	3.7
R197K	$3.0 \times 10^{-4} \pm 0.1 \times 10^{-4}$	4.7 ± 0.6	0.064	1.0×10^3	4.1

[a] Numbers reflect decrease in k_{cat}/K_m parameter relative to wild type; for H120A and H120Q activity decrease was approximated from initial activity estimates as described in the text; for SrtA T180A, L181A, I182A, and I182S k_{cat}/K_m was calculated from the slope of the linear portion of the corresponding Lineweaver−Burk plot from a range of Abz-LPETG-Dap(Dnp) concentrations of 0.33−7.9 mM, 0.29−2.3 mM, 0.3−9.5 mM, and 0.59−13.1 mM, respectively. [b] k_{cat}/K_m values were used to calculate free energies from eq 2 except in the case of H120A and H120Q as indicated above. [c] Not determined.

nucleophile (*4*). However, SrtA C184S retained low levels of activity. Consistent with the essential role of Cys184 in catalysis, k_{cat} was dramatically reduced by over 4 orders of magnitude from 0.69 s^{-1} to 1.9×10^{-5} s^{-1} in SrtA C184S, the lowest measurable k_{cat} for any mutant studied. K_m was also observed to decrease approximately 13-fold from 10.6 mM in wild-type SrtA to 0.79 mM in the C184S mutant. This finding is consistent with the dramatic reduction in k_{cat} seen for this mutant and correlates with the vital role of C184 in the SrtA cleavage of LPXTG-containing substrates. It is also possible that by changing the active site nucleophile from Cys to Ser we produced a SrtA variant that achieves catalysis via an altered mechanism.

In contrast, the kinetic parameters of SrtA D185A and SrtA D186A are very similar to those of the wild-type enzyme. In fact, slight increases are observed in k_{cat} while K_m values appear to decrease slightly, producing an overall increase in catalytic efficiency (k_{cat}/K_m). The significance of this result is unclear and is potentially indicative of a shift in the relative contributions of separate events such as substrate binding or product release to the overall reaction rate. However, it is apparent that neither Asp185 nor Asp186 forms the third member of a Cys-His-Asp catalytic triad. If such were the case, a complete loss of activity upon mutation to alanine would be expected as seen for mutation of the catalytic Asp to alanine in rhinovirus or foot and mouth disease virus 3C protease enzymes (*19*, *20*). In addition, $C^{1/2}_{SUPREX}$ values for the D185A and D186A mutants were unchanged from those of wild-type SrtA (Table 2), indicating that these residues do not contribute to the conformational stability of SrtA.

Perhaps the most revealing information obtained from comparison of kinetic parameters stems from the relative properties of the Arg197 variants. Mutating Arg197 to alanine or to lysine produced negligible decreases in K_m, while k_{cat} decreased by a factor of 10^3 (Table 3) resulting in additive 540- and 1000-fold decreases in catalytic efficiency, respectively. These kinetic parameters differ significantly in magnitude from those measured previously for SrtA R197A and SrtA R197K using an alternate assay; however, Marraffini et al. also observed that the effect of Arg197 is primarily on k_{cat} with K_m essentially unchanged (*6*). Surprisingly, SrtA R197A retained more activity than SrtA R197K despite the conservative nature of the arginine to lysine substitution. It is clear that Arg197 plays a significant role in SrtA catalysis, yet is not absolutely essential as might be expected for a catalytic base (*21*, *22*). Since the effect of mutating Arg197 to alanine or to lysine is on k_{cat} rather than on K_m, as expected for residues involved in transition state stabilization, it is likely that Arg197 functions as an oxyanion hole residue to stabilize negative charge buildup in the transition state and the acyl-enzyme intermediate (*23*).

To more quantitatively address the specific roles played by His120 and Arg197 in SrtA catalysis, the effect of each mutation on the free energy of the transition state preceding substrate cleavage was calculated from the ratio k_{cat}/K_m, or from estimated relative activity measurements in the case of SrtA H120A and H120Q. The energetic contribution of Arg197 to transition state stabilization ($\Delta\Delta G^{\ddagger} = 3.7-4.1$ kcal/mol) correlates well not only with results obtained for carboxypeptidase A and cytomegalovirus protease, which use arginine side chains for oxyanion stabilization, but also for the classical examples of Asn oxyanion stabilization in subtilisin and Gln oxyanion stabilization in papain (*9*, *10*, *24*). In contrast, the values of 6.2−6.8 kcal/mol estimated for SrtA H120A and SrtA H120Q correlate with the value of 7 kcal/mol reported for mutation of the catalytic histidine in trypsin (*25*).

Effect of Cys184 and Arg197 Mutation on pH-Dependence of Catalysis. We previously described a noncanonical reverse protonation mechanism for SrtA in which the pH-dependence of SrtA catalysis is defined by a bell-shaped curve with observed pK_a values of 6.3 and 9.4, likely reflecting the ionization of His120 and Cys184, respectively (*2*). By examining the pH-dependence of SrtA C184S we hoped to see a shift in, or disappearance of, the pK_a value corresponding to Cys184 and unambiguously associate the pK_a of 9.4 with Cys184. We also sought to more directly address the hypothesis posed by Zong and co-workers that Arg197 may serve as a base in SrtA catalysis (*7*). If the pK_a of the basic limb of the pH−rate profile is in fact due to deprotonation of Arg197 rather than Cys184, mutation of Arg197 to alanine or lysine should significantly perturb the overall pH-dependence of catalysis.

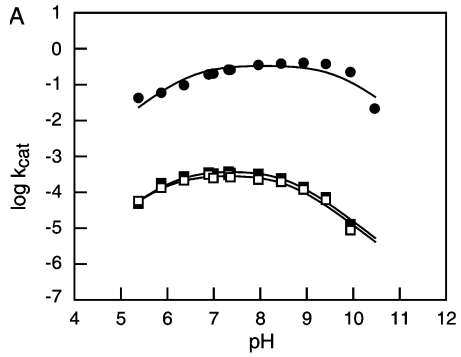

C

Enzyme	pK_{a1}	pK_{a2}
Wild-type	6.5 ± 0.2	9.6 ± 0.2
R197A	6.2 ± 0.1	8.6 ± 0.1
R197K	6.0 ± 0.1	8.6 ± 0.1
C184S	--------	9.7 ± 0.2

FIGURE 3: pH-dependence of k_{cat} for SrtA C184S, R197A, and R197K compared to wild-type enzyme. (A) The log of k_{cat} for wild-type SrtA (●), SrtA R197A (■), and SrtA R197K (□) is plotted as a function of pH. k_{cat} was measured in the presence of 17.8, 15.6, or 16.7 mM Abz-LPETG-Dap(Dnp), respectively. The solid lines drawn through the points were obtained by fitting the data to eq 3. (B) The log of k_{cat} for SrtA C184S (▲) is plotted as a function of pH. Measurements were made in the presence of 10.5 mM Abz-LPETG-Dap(Dnp). Data were fit to eq 4. (C) pK_a values for wild-type SrtA, C184S, R197A, and R197K obtained from eq 3 or 4.

Due to the lengthened reaction times required to observe SrtA C184S, R197A, and R197K activity, the pH stability of SrtA after prolonged incubation over a wide range of pH was assessed. Unfortunately, at the lengthy reaction times required to assay SrtA C184 and R197 variants a steady decline of activity at pH > 8 was observed, with wild-type SrtA activity reduced by about 50% at pH 11.0 (not shown). This decline of SrtA stability at basic pH must be taken into consideration when interpreting the reduced activity of SrtA variants in the basic limb of pH−rate profiles. For wild-type SrtA, R197A, and R197K, the pH-dependence of k_{cat}, shown in Figure 3A, is bell-shaped and well-described by eq 3. In comparison, the curvature of the pH−rate profile for SrtA C184S is not well-defined (Figure 3B), and the data were found to be best fit by eq 4. The pK_a values and associated errors obtained from curve-fitting for each SrtA mutant are listed in Figure 3C.

The pK_a values of 6.5 ± 0.2 and 9.6 ± 0.2 obtained for wild-type SrtA are within error of the previously measured values (*2*). Interestingly, mutation of Arg197 to either alanine or lysine resulted in nearly identical pH−rate profiles; the pK_a of the acidic limb on the pH−rate profile was not significantly altered and the pK_a of the basic limb was depressed by one pH unit relative to wild-type SrtA. That the same decrease is observed whether alanine or lysine is substituted at this position indicates that the positively charged lysine side chain does not accurately mimic the electrostatic effects of arginine and implies specific hydrogen bonding interactions of the Arg197 guanidino group in the enzyme−substrate or transition state complex. Together these results suggest that the catalytically important SrtA ionizations do not reflect the participation of Arg197. If Arg197 was the required base for SrtA catalysis, we would expect that mutation of Arg197 to alanine would result in the disappearance of the basic limb of the pH−rate profile. Additionally, the pK_a of the acidic limb of the pH−rate profile is not altered as would be expected if Arg197 played a role in orienting His120 for catalysis.

Table 4: Solvent Isotope Effects on SrtA Mutants

enzyme	$^{D2O}k_{cat}$	$^{D2O}k_{cat}/K_m$
wild type[a]	0.89 ± 0.01	0.57 ± 0.03
C184S	1.1 ± 0.04	1.48 ± 0.2
D185A	0.93 ± 0.04	0.76 ± 0.002
D186A	1.0 ± 0.04	0.83 ± 0.002
R197A	0.55 ± 0.06	0.6 ± 0.05

[a] From ref 2.

The pH-dependence of SrtA C184S (Figure 3B) did not yield the expected results. We anticipated that mutation of the Cys184 nucleophile would result in the disappearance of the ionization reflected by the basic limb of the pH−rate profile. Instead, no change was observed in the basic limb of the pH−rate profile for SrtA C184S, and the acidic limb was eliminated. However, due to the decline in pH stability of wild-type SrtA at basic pH as well as our inability to measure the activity of SrtA C184S below pH 4.9, we question the accuracy of this result. Additionally, the substitution of Cys184 with the weakly nucleophilic serine side chain possibly produced a SrtA variant with an altered kinetic and/or catalytic mechanism making a direct comparison with the wild-type enzyme inappropriate.

Solvent Isotope Effects Exhibited by SrtA C184S, R197A, D185A, and D186A. Concurrent with our examination of pH-dependence we also examined the effects of bulk solvent substitution on the kinetics of Abz-LPETG-Dap(Dnp) cleavage by several SrtA variants. The calculated isotope effects on k_{cat} and k_{cat}/K_m for SrtA C184S, D185A, D186A, and R197A are listed in Table 4; the values listed for wild-type SrtA are taken from our previous study for comparison (*2*).

We previously attributed the inverse solvent isotope effect exhibited by wild-type SrtA to an effect on the thiol/thiolate equilibrium of Cys184 (*2*). In support of our prior conclusion, mutation of Cys184 to serine produced a significant change in the measured solvent isotope effect. Notably, $^{D2O}k_{cat}/K_m$ increased from 0.57 for wild-type SrtA to 1.48 for SrtA C184S reflecting a shift in the chemistry of substrate cleavage. The normal solvent isotope effect measured for SrtA C184S suggests that chemistry is wholly or partially rate limiting in the cleavage of Abz-LPETG-Dap(Dnp) by SrtA C184S. Instead of representing an equilibrium effect, the observed isotope effect on SrtA C184S could be a kinetic effect reflecting in-flight protons during catalysis. A similar

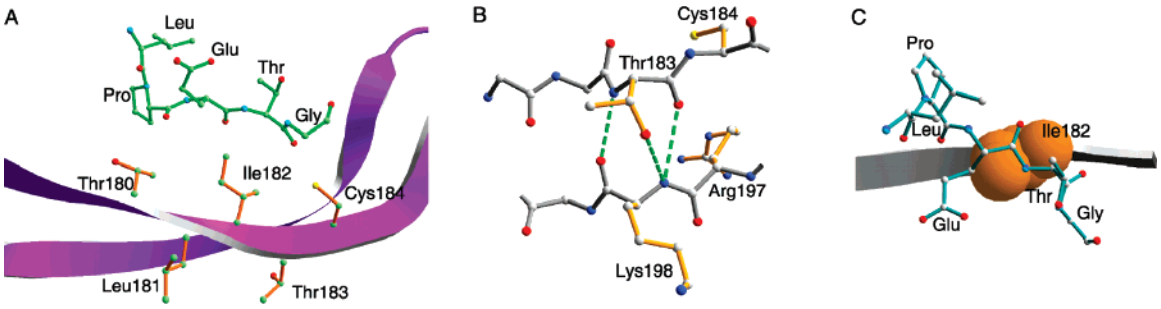

FIGURE 4: Structural interactions of the ^{180}TLITC^{184} motif in SrtA. (A) Position of TLITC motif relative to bound LPETG peptide. The above representation is taken from the crystal structure of *S. aureus* SrtAC184A with LPETG peptide bound (*7*). The side chain of Cys184 is modeled based on its orientation in wild-type SrtA. (B) The side chain hydroxyl of Thr183 can hydrogen bond to the backbone amide nitrogen of Lys198 on the adjacent β-strand. (C) The side chain of Ile182, shown in space-filling representation, appears to interact with bound LPETG peptide through hydrophobic interactions in the region of the Glu−Thr bond.

increase in $^{D2O}k_{cat}/K_m$ from 0.4 to 1.3, reported for SARS 3CL protease upon mutation of the catalytic cysteine residue to serine, was interpreted as being indicative of general base catalysis in the mutant enzyme (*26*).

We have already observed that mutation of Asp185 and Asp186 to alanine failed to produce significant effects on the rate of SrtA-catalyzed transpeptidation (Table 3). Accordingly, the same mutations only produced modest changes in the solvent isotope effect relative to wild-type SrtA, further arguing against a specifically defined catalytic role for these side chains. SUPREX analysis of these mutants suggested that they do not significantly affect the global conformational stability of SrtA. Rather, the small changes observed in the solvent isotope effect could be the result of subtle rearrangements in the SrtA active site upon mutation of Asp185 or Asp186. In turn, these rearrangements could affect the rate of substrate binding or product release relative to chemical transformation, without drastically altering the overall reaction rate.

For SrtA R197A we observed that $^{D2O}k_{cat}/K_m$ was the same as for wild-type SrtA while $^{D2O}k_{cat}$ decreased from 0.89 to a more inverse value of 0.55. The increase in magnitude of the inverse isotope effect on k_{cat} for SrtA R197A signifies that chemistry is more rate-limiting overall than in wild-type SrtA and suggests a role for Arg197 in facilitating bond breaking or making events.

Site-Directed Mutagenesis of the SrtA ^{180}TLITC^{184} Motif. In the past very little emphasis has been placed on identifying residues involved in sortase substrate binding and selectivity. The conserved TLXTC motif found in all sortase isoforms is situated along the β7 strand of SrtA which forms the base of the putative substrate binding pocket. This motif is therefore a prime candidate for involvement in substrate selectivity and definition of active site architecture. The activity of T180A, L181A, I182A, I182S, and T183A SrtA mutants was measured to determine the kinetic parameters k_{cat} and K_m. For SrtA T183A k_{cat} and K_m were easily determined; the values are listed in Table 3. The remaining substitutions within the TLITC motif (T180A, L181A, I182A, and I182S) curiously resulted in SrtA enzymes subject to varying degrees of substrate inhibition. Inhibition was observed above 10.5 mM Abz-LPETG-Dap(Dnp) for SrtA T180A, 2.3 mM for SrtA L181A, 9.5 mM for SrtA I182A, and above 13 mM for SrtA I182S. Increasing the salt concentration from 0.15 to 0.65 M NaCl failed to alleviate inhibition, suggesting that the source of substrate inhibition is not related to electrostatic interaction of the Abz-LPETG-Dap(Dnp) substrate with the SrtA variants. Classic substrate inhibition models failed to accurately describe the data, suggesting a more kinetically complex mechanism and preventing us from obtaining individual k_{cat} and K_m parameters for SrtA T180A, L181A, I182A, and I182S. We instead report estimates of catalytic efficiency calculated from data obtained at low substrate concentrations (Table 3).

Of the residues examined in this study, the most dramatic effect on SrtA catalysis was produced by the mutation of Thr183 to alanine with a 1200-fold decrease in k_{cat} relative to wild-type SrtA. However, the K_m for Abz-LPETG-Dap(Dnp) was unaffected. While initially unexpected, changes in the affinity of SrtA T183A for the Abz-LPETG-Dap(Dnp) substrate may not be apparent in K_m as they may be masked by the dramatic decrease observed in k_{cat}. Alternatively, it is possible that Thr183 is not directly involved in substrate binding, as the side chain of Thr183 is positioned away from the interior of the substrate binding pocket (Figure 4A). Interestingly, the $C^{1/2}_{SUPREX}$ value for this mutant was also unchanged from that of wild-type SrtA, suggesting that Thr183 is not critical for maintaining global conformational stability. Further inspection of the SrtA crystal structure reveals that Thr183 has the potential to form three hydrogen bonds with the backbone of Lys198 on the adjacent β8 strand (Figure 4A). Notably, the hydroxyl group of the Thr183 side chain is within hydrogen bonding distance of the backbone carboxyl group of Lys198. Mutation of Thr183 to alanine would eliminate this hydrogen bond, and an alanine residue at this position might be free to rotate and disrupt the position of the adjacent Cys184 nucleophile, leading to the observed decrease in k_{cat} for this mutant.

Although the estimated effects of Thr180, Leu181, and Ile182 mutation on catalytic efficiency are relatively modest (7- to 74-fold decrease), the inhibitory effects of high substrate concentrations on these variants imply that these residues could be determinants of productive substrate binding. For all four of these mutants $C^{1/2}_{SUPREX}$ values (Table 2) were also significantly decreased relative to wild-type SrtA, indicative of a reduction in conformational stability. Furthermore, the magnitude of the decrease in $C^{1/2}_{SUPREX}$ correlates with the degree of substrate inhibition observed; the severity of substrate inhibition was greatest for SrtA L181A, also the variant for which the largest decrease in $C^{1/2}_{SUPREX}$ was observed. Together, these findings are consistent with the above suggestion that substrate

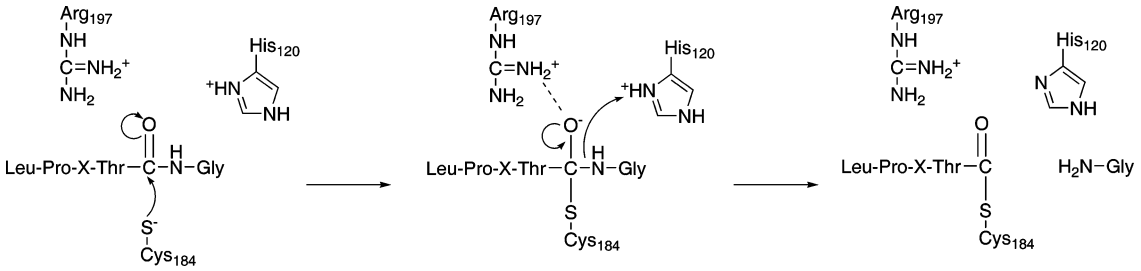

FIGURE 5: Revised reverse protonation model for SrtA catalysis. The LPXTG substrate binds to active SrtA in which Cys184 and His120 are reverse protonated; this represents a minor fraction of total SrtA population. The nucleophilic Cys184 thiolate attacks the carbonyl of the scissile Thr−Gly bond to result in the formation of a short-lived tetrahedral oxyanion intermediate which is stabilized by interaction with the positively charged side chain of Arg197. Protonation of the leaving group facilitates collapse of the intermediate and formation of the acyl-enzyme.

inhibition could be the result of nonproductive substrate binding, due to disruption of the SrtA active-site structure.

Examining the structural interactions of the Thr180, Leu181, and Ile182 side chains in the vicinity of the SrtA active site provides some further insight as to the cause of the effects observed upon mutation of these residues. In the crystal structure of SrtA with LPETG peptide bound, Ile182 appears to interact with the peptide through hydrophobic interactions in the region of the Glu−Thr bond (Figure 4B). It is possible that the observed decrease in SrtA activity is the manifestation of a decrease in substrate binding affinity produced upon removal of the Ile182 side chain. Since the Ile182 side chain appears to interact with the LPETG peptide through hydrophobic interaction, it is not surprising that mutation of Ile182 to a more hydrophilic serine caused a larger decrease in activity than did the corresponding alanine substitution. The function of the naturally occurring serine at this position in *S. aureus* SrtB could similarly facilitate the binding of the more hydrophilic NPQTN sequence recognized by sortase B enzymes. Mutation of Thr180 and Leu181 produced less dramatic effects on sortase activity, consistent with their positioning toward the N-terminal end of the β7 strand. The side chain of Thr180 may be interacting with the proline residue of the peptide substrate; however, the side chain of Leu181 extends from the opposite side of the strand (Figure 4C). The disruption of structural hydrophobic packing interactions between Leu181 and hydrophobic side chains of the neighboring β4 and β8 strands may affect the shape of the substrate binding pocket and the conformational stability of the protein. The substrate inhibition observed for SrtA T180A, although less severe, may likewise be due to local structural rearrangements resulting from the disruption of hydrogen bonding interactions between Thr180 and Asn114 (not shown). Alternatively, inhibition could be the result of nonproductive substrate binding in the slightly enlarged groove formed upon removal of the threonine side chain (*27*).

A Revised Reverse Protonation Model for SrtA Catalysis. Despite the recognized need for a clear understanding of SrtA catalytic mechanism, recent literature has been clouded with controversy regarding the proposed functional roles of key active-site residues in sortase enzymes. Previous results obtained in studies of wild-type SrtA from *S. aureus* support a reverse protonation model for SrtA catalysis in which a minor portion of Cys184 and His120 exist in the active thiolate and imidazolium forms required for catalysis (*2*). However, this model left the role of Arg197 in SrtA catalysis undefined and did not adequately address the possible participation of Asp185 or Asp186. The combination of site-directed mutagenesis, pH−rate profiles, and solvent isotope effects reported in this study is consistent with a reverse protonation model for SrtA catalysis. We argue against the direct participation of Asp185 or Asp186 in substrate processing, and provide evidence that Arg197 functions to stabilize the oxyanion transition state. In addition, we have refuted the previous claim that the inactivity of SrtA H120A can be explained by loss of SrtA structural stability, and have demonstrated that Cys184 is the source of the inverse solvent isotope effect observed for wild-type SrtA.

In light of these new findings, our previously proposed mechanistic model is redrawn in Figure 5 to include the participation of Arg197 in transition state stabilization. In this model, a minor fraction of the total SrtA population exists in an active reverse protonated form (Cys184 thiolate and His120 imidazolium). The LPXTG substrate binds to the active site through interactions with amino acid side chains, including Thr180 and Ile182, located along the β7 and β8 strands and the β6−β7 loop (not shown). The nucleophilic Cys184 thiolate attacks the carbonyl of the scissile Thr−Gly bond in the LPXTG-containing substrate to form a tetrahedral oxyanion transition state. The negatively charged transition state is stabilized by interaction with the positively charged guanidinium side chain of Arg197. His120 is then hypothesized to protonate the substrate leaving group, facilitating the collapse of the tetrahedral intermediate and formation of the acyl-enzyme. Since acylation is rate-limiting overall in SrtA catalyzed transpeptidation, events subsequent to acyl-enzyme formation have not been directly examined in the current study. In addition to stabilization of the oxyanion in the transition state, it is possible that Arg197 also facilitates the departure of the substrate leaving group or activates the incoming pentaglycine-branched lipid II nucleophile.

We now have a more precise picture of the catalytic mechanism of SrtA acylation by LPETG-containing peptides that will assist in the development of more potent SrtA inactivators. Nevertheless, we still do not understand the complement of factors that govern substrate selection and binding. Thr180, Leu181, and Ile182 clearly play a role, either directly or indirectly, in maintaining the shape of the SrtA substrate-binding pocket, while Thr183 most likely affects the positioning of the Cys184 or Arg197 side chains. The contribution of other surrounding residues to LPXTG binding and recognition remains to be elucidated.

REFERENCES

1. Paterson, G. K., and Mitchell, T. J. (2004) The biology of Gram-positive sortase enzymes, *Trends Microbiol. 12*, 89−95.
2. Frankel, B. A., Kruger, R. G., Robinson, D. E., Kelleher, N. L., and McCafferty, D. G. (2005) Staphylococcus aureus Sortase Transpeptidase SrtA: Insight into the Kinetic Mechanism and Evidence for a Reverse Protonation Catalytic Mechanism, *Biochemistry 44*, 11188−11200.
3. Huang, X., Aulabaugh, A., Ding, W., Kapoor, B., Alksne, L., Tabei, K., and Ellestad, G. (2003) Kinetic mechanism of *Staphylococcus aureus* sortase SrtA, *Biochemistry 42*, 11307−11315.
4. Ton-That, H., Mazmanian, S. K., Alksne, L., and Schneewind, O. (2002) Anchoring of surface proteins to the cell wall of *Staphylococcus aureus*. Cysteine 184 and histidine 120 of sortase form a thiolate-imidazolium ion pair for catalysis, *J. Biol. Chem. 277*, 7447−7452.
5. Ilangovan, U., Ton-That, H., Iwahara, J., Schneewind, O., and Clubb, R. T. (2001) Structure of sortase, the transpeptidase that anchors proteins to the cell wall of *Staphylococcus aureus*, *Proc. Natl. Acad. Sci. U.S.A. 98*, 6056−6061.
6. Marraffini, L. A., Ton-That, H., Zong, Y., Narayana, S. V., and Schneewind, O. (2004) Anchoring of surface proteins to the cell wall of *Staphylococcus aureus*. A conserved arginine residue is required for efficient catalysis of sortase A, *J. Biol. Chem. 279*, 37763−37770.
7. Zong, Y., Bice, T. W., Ton-That, H., Schneewind, O., and Narayana, S. V. (2004) Crystal structures of *Staphylococcus aureus* sortase A and its substrate complex, *J. Biol. Chem. 279*, 31383−31389.
8. Zong, Y., Mazmanian, S. K., Schneewind, O., and Narayana, S. V. (2004) The structure of sortase B, a cysteine transpeptidase that tethers surface protein to the *Staphylococcus aureus* cell wall, *Structure 12*, 105−112.
9. Phillips, M. A., Fletterick, R., and Rutter, W. J. (1990) Arginine 127 stabilizes the transition state in carboxypeptidase, *J. Biol. Chem. 265*, 20692−20698.
10. Liang, P. H., Brun, K. A., Feild, J. A., O'Donnell, K., Doyle, M. L., Green, S. M., Baker, A. E., Blackburn, M. N., and Abdel-Meguid, S. S. (1998) Site-directed mutagenesis probing the catalytic role of arginines 165 and 166 of human cytomegalovirus protease, *Biochemistry 37*, 5923−5929.
11. Kruger, R. G., Otvos, B., Frankel, B. A., Bentley, M., Dostal, P., and McCafferty, D. G. (2004) Analysis of the substrate specificity of the *Staphylococcus aureus* sortase transpeptidase SrtA, *Biochemistry 43*, 1541−1551.
12. Mazmanian, S. K., Ton-That, H., Su, K., and Schneewind, O. (2002) An iron-regulated sortase anchors a class of surface protein during *Staphylococcus aureus* pathogenesis, *Proc. Natl. Acad. Sci. U.S.A. 99*, 2293−2298.
13. Liew, C. K., Smith, B. T., Pilpa, R., Suree, N., Ilangovan, U., Connolly, K. M., Jung, M. E., and Clubb, R. T. (2004) Localization and mutagenesis of the sorting signal binding site on sortase A from *Staphylococcus aureus*, *FEBS Lett. 571*, 221−226.
14. Pallen, M. J., Lam, A. C., Antonio, M., and Dunbar, K. (2001) An embarrassment of sortases - a richness of substrates?, *Trends Microbiol. 9*, 97−102.
15. Dramsi, S., Trieu-Cuot, P., and Bierne, H. (2005) Sorting sortases: a nomenclature proposal for the various sortases of Gram-positive bacteria, *Res. Microbiol. 156*, 289−297.
16. Gill, S. C., and von Hippel, P. H. (1989) Calculation of protein extinction coefficients from amino acid sequence data, *Anal. Biochem. 182*, 319−326.
17. Ghaemmaghami, S., Fitzgerald, M. C., and Oas, T. G. (2000) A quantitative, high-throughput screen for protein stability, *Proc. Natl. Acad. Sci. U.S.A. 97*, 8296−8301.
18. Kruger, R. G., Dostal, P., and McCafferty, D. G. (2004) Development of a high-performance liquid chromatography assay and revision of kinetic parameters for the *Staphylococcus aureus* sortase transpeptidase SrtA, *Anal. Biochem. 326*, 42−48.
19. Cheah, K. C., Leong, L. E., and Porter, A. G. (1990) Site-directed mutagenesis suggests close functional relationship between a human rhinovirus 3C cysteine protease and cellular trypsin-like serine proteases, *J. Biol. Chem. 265*, 7180−7187.
20. Grubman, M. J., Zellner, M., Bablanian, G., Mason, P. W., and Piccone, M. E. (1995) Identification of the active-site residues of the 3C proteinase of foot-and-mouth disease virus, *Virology 213*, 581−589.
21. Sanchez-Torres, P., Visser, J., and Benen, J. A. (2003) Identification of amino acid residues critical for catalysis and stability in *Aspergillus niger* family 1 pectin lyase A, *Biochem. J. 370*, 331−337.
22. Doherty, M. K., Pealing, S. L., Miles, C. S., Moysey, R., Taylor, P., Walkinshaw, M. D., Reid, G. A., and Chapman, S. K. (2000) Identification of the active site acid/base catalyst in a bacterial fumarate reductase: a kinetic and crystallographic study, *Biochemistry 39*, 10695−10701.
23. Bryan, P., Pantoliano, M. W., Quill, S. G., Hsiao, H. Y., and Poulos, T. (1986) Site-directed mutagenesis and the role of the oxyanion hole in subtilisin, *Proc. Natl. Acad. Sci. U.S.A. 83*, 3743−3745.
24. Menard, R., and Storer, A. C. (1992) Oxyanion hole interactions in serine and cysteine proteases, *Biol. Chem. Hoppe-Seyler 373*, 393−400.
25. Phillips, M. A., and Fletterick, R. J. (1992) Proteases, *Curr. Opin. Struct. Biol. 2*, 713−720.
26. Huang, C., Wei, P., Fan, K., Liu, Y., and Lai, L. (2004) 3C-like proteinase from SARS coronavirus catalyzes substrate hydrolysis by a general base mechanism, *Biochemistry 43*, 4568−4574.
27. Segel, I. H. (1975) *Enzyme kinetics: behavior and analysis of rapid equilibrium and steady-state systems*, Wiley Classics Library Edition, Wiley, New York.

BI700448E